Materials Science Forum *Online: 2006-01-15*
ISSN: 1662-9752, Vols. 503-504, pp 793-798
doi:10.4028/www.scientific.net/MSF.503-504.793

Evaluation of a Ni-20Cr Alloy Processed by Multi-axis Forging

R. DiDomizio[1,a], M.F. Gigliotti[1,b], J.S. Marte[1,c], PR. Subramanian[1,d], V. Valitov[2,e]

[1]GE Global Research, One Research Circle, Niskayuna, NY, 12309 USA

[2]Institute for Metals Superplasticity Problems of Russian Academy of Sciences, 39, ul. Stepana Khalturina, Ufa 450001, Republic of Bashkortostan, Russia

[a]didomizr@crd.ge.com, [b]gigliotti@crd.ge.com, [c]marte@crd.ge.com, [d]subrampr@crd.ge.com, [e]gensal@imsp.da.ru

Keywords: Multi-axis forging, Nickel-chromium, Grain growth, High-cycle fatigue

Abstract. This paper discusses the development of a novel processing route to produce ultra fine-grain bulk alloy forgings; the microstructural response of these forgings to thermal exposure; and the comparison of mechanical properties to those from conventionally processed material. A Ni-20Cr [wt%] alloy was processed by near-isothermal multi-axis forging to a grain size of approximately 1 μm. A heat-treatment study over the range 900 to 1200°C was conducted to determine the resultant grain size as a function of time and temperature. Tensile properties were measured at room temperature, 500°C, and 930°C. High-cycle fatigue properties were measured at room temperature. The room-temperature tensile strength was approximately 2.5 times greater than that of conventionally processed Ni-20Cr. Fatigue data showed that the room-temperature high-cycle fatigue run-out stress was greater than 100% of the yield stress.

Introduction

The Hall-Petch relationship predicts that the strength of a material increases with the inverse square root of the grain size [1]. As a result, a great deal of effort has been dedicated to creating nanostructured and ultrafine-grained materials using severe plastic deformation (SPD) to significantly increase the strength of engineering materials. Two common SPD methods used to create these fine-grained structures are equal-channel angular extrusion (ECAE) and high-pressure torsion (HPT) [2,3,4]. However, both of these methods have drawbacks for industrialization. ECAE requires special tooling that is expensive and has not yet been scaled up to a size that makes it viable for widespread industrial use. Similarly, HPT is a small-scale process that would be difficult to scale up and make industrially viable. HPT also produces a strain gradient that results in an increasing degree of refinement from the central axis of rotation to the outside radius. Thus, none of these processes is immediately available for creating bulk fine-grained material.

A third SPD process, that does not require any special tooling and is immediately available for industrial use, is multi-axis forging. In this process, a billet undergoes a conventional forging operation under carefully controlled temperatures and strain rates. Between each forging pass, the billet is reoriented such that each subsequent forging step is carried out in a direction orthogonal to the previous two. A schematic of this process is shown in Fig. 1. By reorienting the billet between each forging pass, strain is accumulated without reducing the cross section to such a degree that the billet becomes unusable for an industrial application.

SPD processing has been carried out on many pure metals, including aluminum, titanium, copper, and their respective alloys. Zhilyaev et al. have studied pure nickel extensively, including ECAE and HPT studies evaluating grain growth kinetics and microstructural evolution [5,6,7]. However, little published work on SPD processing of nickel-based alloys can be found in the literature [8].

The present study was designed to provide initial results on grain growth kinetics and mechanical properties of a simple nickel-based alloy that has been severely deformed by multi-axis forging.

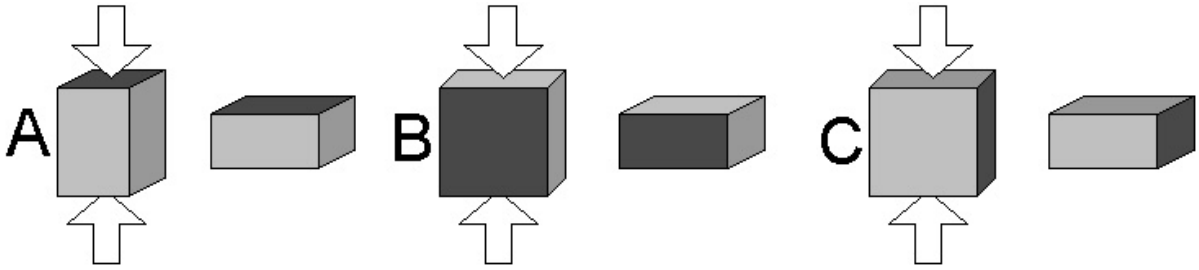

Fig. 1: Schematic of multi-axis forge processing

Experimental Procedures

The alloy used was nominally Ni-20Cr [wt%] with small alloying additions of Al, Zr, Fe, Co, Mn, and Si. The starting material was fully recrystallized with a grain size range of 25 to 52 μm. The multi-axis forging was performed at the Institute for Metals Superplasticity Problems of Russian Academy of Sciences, Ufa, Russia. The processing temperature range was 700°C to 800°C and pre-heated forging dies were used to achieve near-isothermal forging conditions. Forging was conducted in a strain rate range of 10^{-3} to 10^{-4} s^{-1}. No cracking was seen on the sample surfaces following forging. The as-forged billets varied in geometry, but they were roughly 2.5 cm square in cross section and 15 cm in length.

Heat-treatment studies were conducted in a quartz tube under flowing argon. Samples were sectioned from the forged billets to dimensions of 1 cm x 1 cm x 0.5 cm. The samples were either plunged at temperature or ramped to the desired temperature in a specified amount of time. Upon reaching the desired temperature, the samples were held at that temperature for two hours and then immediately water-quenched.

After confirming that the hardness measurements on the longitudinal and transverse faces were statistically identical, all further measurements were made on the transverse face. Macrohardness measurements were obtained on both a Rockwell C and Rockwell B scale and were converted to a Vickers scale via ASTM standard E140 for nickel and nickel alloys to allow a direct comparison.

Tensile and fatigue specimens were machined from the as-forged billets so that the test specimens were aligned with the long axis of the billet. The round, button-head tensile specimens had a uniform gage length of 9.0 mm and tests were conducted in a screw-driven machine with a crosshead displacement of 0.51 mm/min. The high-temperature tensile samples were ramped to the test temperature and allowed to equilibrate for 30 minutes prior to the beginning of each test. Round, button-head high-cycle fatigue (HCF) specimens were tested under load control with a 30 Hz sine wave. The minimum load was varied with the maximum load to keep the stress ratio, R, constant at 0.05. All HCF tests were conducted at room temperature. Tests were considered to be run-outs if the sample lasted greater than ten million cycles.

Experimental Results and Discussion

Microstructure Evaluation. Optical and TEM micrographs of the as-forged microstructure are shown in Figs. 2 and 3, respectively. The optical micrograph shows equiaxed grains developed during the forging process. The TEM micrograph shows a dislocated central grain with a slip band and a deformation twin. TEM analysis also showed the presence of a low volume fraction of second-phase particles. Zone axis diffraction patterns showed the presence of $Cr_{23}C_6$ carbides ranging in size from 100 nm to 500 nm and energy-filtered TEM images showed the presence of Cr-Ti-Mg bearing nitrides ranging in size from 50 to 100 nm.

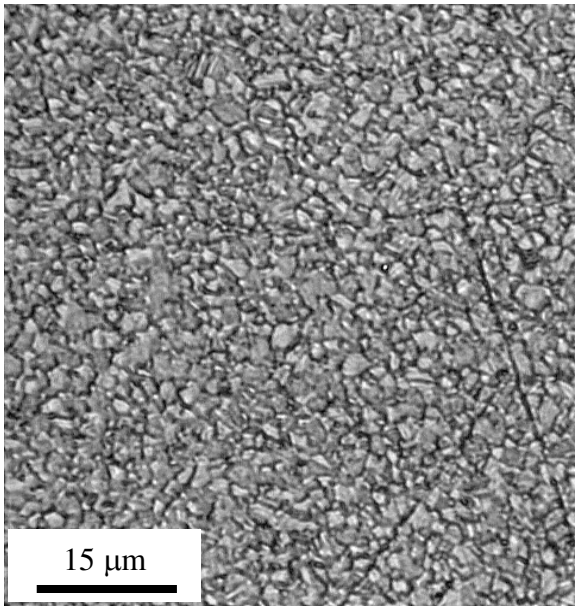

Fig. 2: Optical micrograph from polished and etched planar cross-sections of as-forged Ni-20Cr

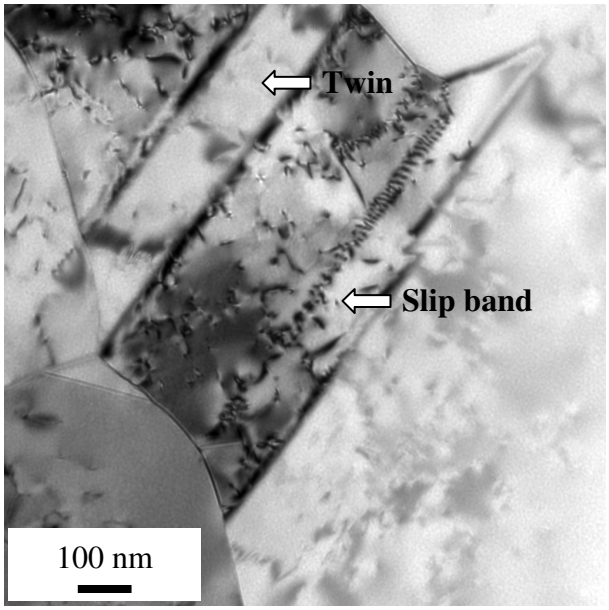

Fig. 3: TEM bright field image of as-forged Ni-20Cr; note presence of deformation twin and slip band

Grain Growth Kinetics. A matrix of dwell temperatures and ramp times, shown in Fig. 4, was chosen to investigate the grain growth kinetics of the as-forged material. The samples were held at the desired temperature for two-hours. Prior to exposure, each of the nine samples had a section removed for initial grain size and hardness analysis. The grain size was determined by using the intercept method described in ASTM standard E112. The mean hardness for these nine samples was 296 ± 3 H_V and the mean grain size was 1.3 ± 0.2 μm.

Fig. 4 shows the mean room-temperature hardness and mean grain size for each of the nine exposure conditions. The data showed that as the temperature increased, the grain size also increased. This grain growth was accompanied by an expected decrease in hardness. However, as the ramp time increased from zero (a plunge at temperature) to a 16-hour ramp, there was very little change in grain size or hardness. An analysis of variance showed that at a common temperature, the grain size and hardness were statistically indistinguishable for the various ramp times at a 95% confidence level. However, individual T-tests showed that at a 90% confidence level grain sizes at several exposure conditions were statistically differentiable. These statistical calculations lead to the speculation that the varying ramp times chosen did not vary over a large enough range in time at temperature to allow a distinguishable difference in grain size and hardness to be measured. To confirm this hypothesis, a common ramp time should be chosen and the dwell time at temperature varied.

The Hall-Petch relationship can be written as

$$\sigma_0 = \sigma_i + k \cdot d^{-1/2}, \tag{1}$$

where σ_0 is the yield stress, σ_i is the Peierls or frictional stress, k is the Hall-Petch slope, and d is the grain size [1]. The Vickers hardness values were used to estimate the yield strength by the relationship $\sigma_y = H_V/2.5$ so that a Hall-Petch relationship showing yield strength as a function of the inverse of the square root of the grain size could be constructed as shown in Fig. 5. Each data point in Fig. 5 represents an average of at least three measurements and the regression of these mean values fits very well with an R^2 value of 98%. From the Hall-Petch plot it was found that σ_i was

equal to 254 ± 0.01 MPa and k was equal to 622 ± 0.02 MPa/μm$^{1/2}$. Because of the excellent regression fit to the experimental data, 95% confidence intervals are indistinguishable from the linear regression line and are not plotted in Fig 5.

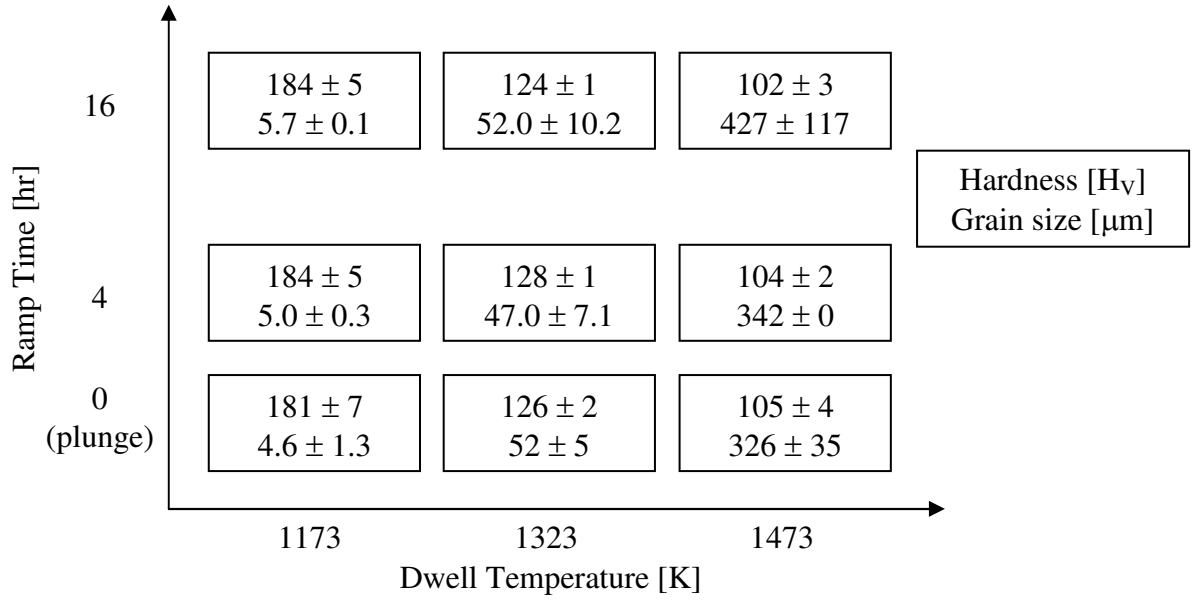

Fig. 4: Hardness and grain size results from the heat-treatment matrix

The results of the heat-treatment study were also used to produce an Arrhenius plot, shown in Fig. 6, relating grain size and temperature. An exponential regression was fit to each of the three different data sets corresponding to the different heating rates. The fits correspond to the equation

$$d = C_0 \exp\left(\frac{Q}{RT}\right), \tag{2}$$

where C_0 is a constant, Q is the activation energy, R is the universal gas constant, and T is the absolute temperature. The exponential fit for each data set had an R^2 value greater than 99%. From each of the three fits, the activation energy was calculated as shown in Table 1.

Table 1. Calculated activation energies for grain growth in Ni-20Cr

Ramp Time	Activation Energy [kJ/mol]
Plunge	204.2 ± 0.7
4-hr Ramp	201.9 ± 0.8
16-hr Ramp	206.0 ± 1.0

The activation energies calculated from the exponential regressions were lower than the activation energy for diffusion in pure nickel, which is reported to be approximately 282 kJ/mol in the temperature range of interest [9,10]. However, chromium alloying additions increase the nickel diffusivity as predicted by Shewmon [11] and, as a result, the activation energy for nickel is reduced to 264 kJ/mol for Ni-20Cr as shown experimentally by Ugaste [12]. This value is 60 kJ/mol higher than that calculated in this study. Zhilyaev et al. reported the activation energy for grain boundary diffusion in pure nickel to be 103 kJ/mol, which is approximately 100 kJ/mol lower than the activation energy calculated [5]. Thus, the activation energy for grain growth calculated in

this study does not conclusively support either bulk diffusion or grain boundary diffusion as the primary mechanism for grain growth.

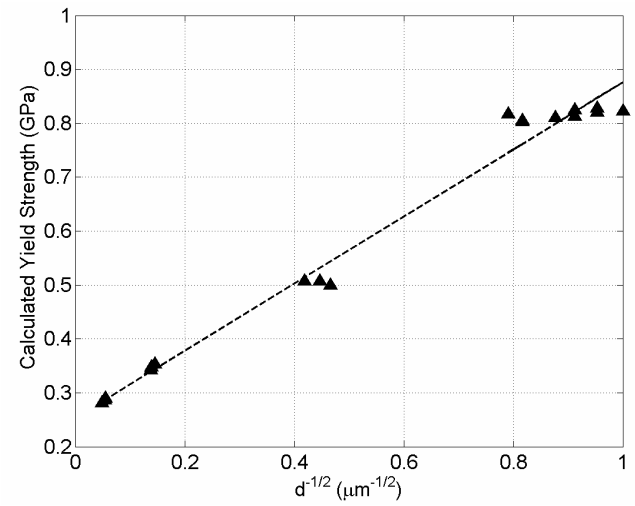

Fig. 5: Hall-Petch plot of multi-axis forged Ni-20Cr

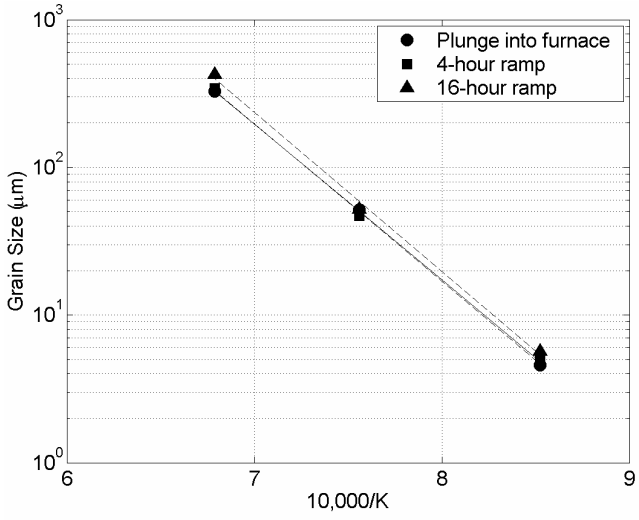

Fig. 6: Arrhenius relationship between grain growth and temperature

Mechanical Properties. Tensile experiments were conducted on both multi-axis forged samples and conventionally wrought Ni-20Cr samples, which had an average grain size of 64 ± 16 μm. Fig. 7 shows both the multi-axis forged and wrought experimental data, along with a reference curve of experimental data for Ni-20Cr [13].

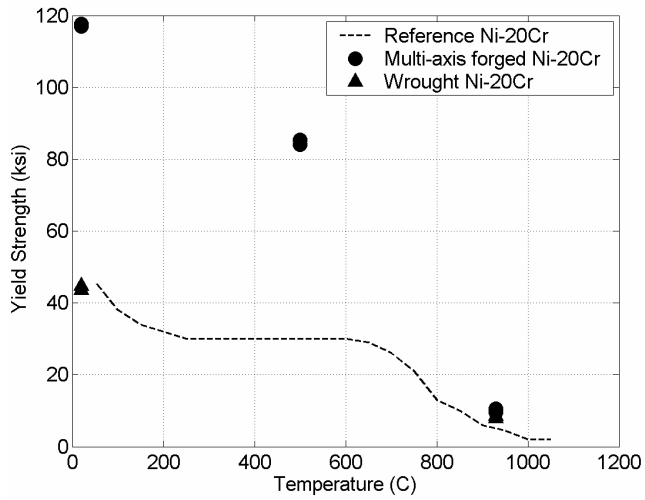

Fig. 7: Tensile properties of multi-axis forged and wrought Ni-20Cr

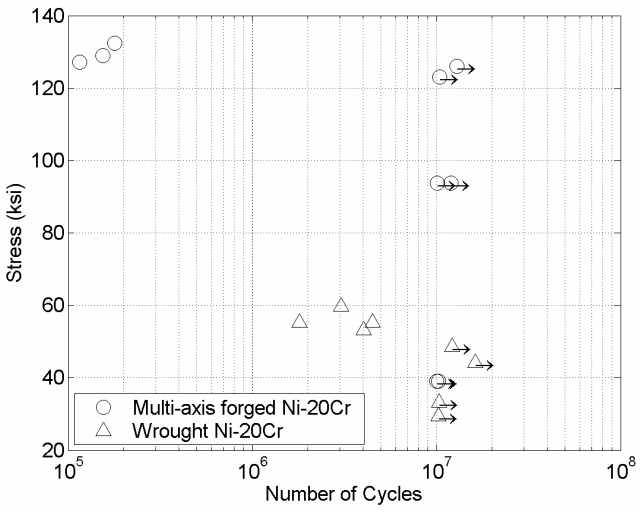

Fig. 8: S-N plot of multi-axis forged and wrought Ni-20Cr

At room temperature and 500°C, the yield strength of the multi-axis forged Ni-20Cr was more than 2.5 times that of the conventionally processed Ni-20Cr. The room-temperature elongation to failure of the multi-axis forged material was 30%, while for the conventionally processed Ni-20Cr elongation to failure was 47%. Thus, the large increase in room temperature yield strength was accompanied by a decrease in elongation to failure. At 930°C, the yield strengths of the two materials were statistically indistinguishable at a 95% confidence level, consistent with the grain growth in the multi-axis forged material.

The room-temperature high-cycle fatigue test results (Fig. 8) showed run-outs in the multi-axis forged Ni-20Cr samples at up to 107.5% of the yield strength. Failure at 110% of the yield strength occurred after 154,000 cycles. The conventionally forged Ni-20Cr samples also had run-outs at stresses exceeding the tensile yield stress. Failure at 120% of the yield strength occurred after 4 million cycles.

Summary and Conclusions

1) Multi-axis forging was effective in reducing the average grain size from approximately 40 μm to an average of 1.3 μm. Optimization of the multi-axis forging process may further decrease the grain size.
2) Activation energy calculations fell between the literature values for bulk diffusion and grain boundary diffusion activation energies. Thus, while the activation energies calculated in this study are in the correct range, they cannot conclusively point to a mechanism driving grain growth.
3) Yield strength, as converted from hardness measurements, followed a Hall-Petch dependence.
4) The higher yield strength of the multi-axis forged Ni-20Cr relative to the conventionally forged Ni-20Cr is retained to a temperature of at least 500°C. At 930°C, the yield strengths are statistically indistinguishable.
5) The multi-axis forged material exhibited a significantly higher run-out stress than the wrought material.

Acknowledgements

The authors would like to acknowledge M. Gilhooly, C. Canestraro, and J. Thompson for the mechanical testing; T. Barbuto for the metallography; J. Grande for the image analysis, and M. Larsen for the TEM analysis. The authors would also like to acknowledge Margaret Blohm (Project Leader Nanotechnology) for providing funding for this project.

References

[1] G. E. Dieter, *Mechanical Metallurgy* (McGraw-Hill, New York, 1986), p 189.
[2] V. M. Segal: Mat. Sci. & Eng. A Vol 197 (1995), p 157.
[3] S. L. Semiatin, D. P. Delo, E. B. Shell: Acta. Mater. Vol 48 (2000), p 1841.
[4] A. Vorhauer, R. Pippan: Scripta Mater. Vol 51 (2004), p 921.
[5] A. P. Zhilyaev, G. V. Nurislamova, M. D. Baro, R. S. Valiev, T. G. Langdon: Met. Trans. A. Vol 33A (2002), p 1865.
[6] A. P. Zhilyaev, B. K. Kim, J. A. Szpunar, M. D. Baro, T. G. Langdon.: Mat. Sci. & Eng. A. Vol 391 (2005), p 377.
[7] A. P. Zhilyaev, G. V. Nurislamova, B. K. Kim, M. D. Baro, J. A. Szpunar, T. G. Langdon: *Nanomaterials by Severe Plastic Deformation*. (TMS, Pennsylvania, 2004), p 387.
[8] K. Oh-ishi, Z. Horita, D. J. Smith, R. S. Valiev, M. Nemoto, T. G. Langdon: J. of Mat. Research. Vol 14 (1999), p 4200.
[9] C. J. Smithells, *Metals Reference Book 5th Edition* (Butterworths, London, 1976), p 869.
[10] H. Mehrer, *Landolt-Bornstein Numerical Data & Functional Relationships in Science & Technology, V26, Diffusion in Solid Metals & Alloys* (Springer-Verlag, 1990), p 52.
[11] P. Shewmon, *Diffusion in Solids* (TMS, Warrendale, 1989), p 147.
[12] Yu. E. Ugaste: Fiz. Metal Metalloved. Vol 24 (1967), p 442.
[13] J. Davis, *ASM Specialty Handbook: Heat Resistant Materials* (ASM International, Materials Park, 1997), p 386.